



Journal of Applied and Computational Mechanics



Research Paper

Improving the linear stability of the visco-elastic Beck's beam via piezoelectric controllers

Arnaldo Casalotti^{1,2}, Francesco D'Annibale^{1,2}*

¹Department of Civil, Construction-Architectural and Environmental Engineering, University of L'Aquila, 67100 L'Aquila, Italy, Email: arnaldo.casalotti@univaq.it

²International Research Center on Mathematics and Mechanics of Complex Systems, University of L'Aquila, 67100, L'Aquila, Italy, Email: francesco.dannibale@univaq.it

Received May 18 2020; Revised August 04 2020; Accepted for publication August 07 2020.

Corresponding author: Francesco D'Annibale (francesco.dannibale@univaq.it)

© 2021 Published by Shahid Chamran University of Ahvaz

Abstract. Control strategies for the visco-elastic Beck's beam, equipped with distributed piezoelectric devices and suffering from Hopf bifurcation triggered by a follower force, are proposed in this paper. The equations of motion of the Piezo-Electro-Mechanical (PEM) system are derived through the Extended Hamilton Principle, under the assumption that the piezoelectric patches are shunted to the so-called zero-order network and zero-order analog electrical circuit. An exact solution for the eigenvalue problem is worked out for the PEM system, while an asymptotic analysis is carried out to define three control strategies, recently developed for discrete PEM systems, that are here adapted to improve the linear stability of the visco-elastic Beck's beam. An extensive parametric study on the piezo-electrical quantities, based on an exact linear stability analysis of the PEM system, is then performed to investigate the effectiveness of the controllers.

Keywords: Piezo-Electro-Mechanical systems, Vibration Control, Linear Stability Analysis, Hopf bifurcation, Beck's beam.

1. Introduction

Structural vibration mitigation is an interesting topic, that has been widely investigated due to its relevance in various fields of engineering applications. Among the most used control devices, there are the so-called Tuned Mass Damper (TMD) [1, 2, 3, 4, 5, 6, 7, 8, 9, 10, 11, 12] and the Nonlinear Energy Sink (NES) [13, 14, 15, 16, 17]. Both TMD- and NES-based control is grounded on the idea that structural vibration mitigation can be obtained when the response of the controller (secondary system) resembles that of the structure (primary system): this is known as the 'principle of similarity' [18]. Indeed, the frequency of the TMD is closely tuned to that of the primary system, thus entailing the splitting of one peak of the frequency-response curve into two lower peaks and, accordingly, a reduction of the response of the primary system to the external resonant excitations. In the NES-based control similarity is achieved by connecting the device to the primary system through an essentially nonlinear elastic spring, thus rendering it able to self-tune itself to the requested frequency, and allowing it to work in a larger frequency range with respect to TMD.

Since their first introduction in the early 1990s, piezoelectric materials have received great attention from researchers and related industrial applications have increased over the years. They have been exploited also as metamaterials to obtain smart systems [19, 20], with application as well in the context of civil and industrial engineering structures [21]. Piezoelectric controllers are usually designed according to the principle of similarity, i.e. by tuning the resonance(s) of the electric circuit, which is shunted to piezoelectric device(s), to one (or more) natural frequencies of the mechanical system. Therefore, they could behave as a TMD, or as an array of distributed TMDs, with the advantage of a simpler tuning procedure and less added weight than classic TMD. In [22, 23, 24, 25, 26, 27, 28, 29, 30, 31] Piezo-Electro-Mechanical (PEM) systems are built up, by attaching arrays of piezoelectric patches to primary systems and designing 'similar' analogous circuits. Due to the electro-mechanical coupling, the mechanical energy is allowed to migrate to the electrical circuit and then dissipated by optimized resistors. In particular in [31], different analogous circuits are formalized, by properly changing the space and time derivatives governing the flux-linkage equation.

Research on vibration mitigation is mainly oriented to analyze the behavior of controlled *non-autonomous* systems, subjected then to external excitation, while further efforts may still be conducted to understand the response of controlled *autonomous* systems under the action of non-conservative forces, of velocity- and/or position-dependent type. Several applications of structures, ranging from aerospace to sport engineering, indeed, are subjected to this class of actions, e.g.: aircrafts, arrows, wings, sails, jets and rocket motors, tall buildings, flexible pipes, vehicle brakes, javelins and arrows. Moreover, autonomous systems, loaded by non-conservative forces of positional type such as follower forces, i.e. so-called 'circulatory systems', may exhibit the Ziegler's paradox (see, e.g., [32, 33, 34, 35, 36, 37, 38, 39, 40, 41]). This phenomenon consists in a destabilizing effect of damping, that manifests itself through a finite reduction of the Hopf critical load of a circulatory system, when a small damping is added to it.

Piezoelectric control of autonomous systems, under follower forces is developed in [42, 43, 44, 45, 46, 47]. In [42, 43] piezoelectric devices are attached to a column and to a viscoelastic plate, respectively, and their effect in increasing the systems stability is discussed. The principle of similarity was not actually applied, since the non-conservative effect, due to the follower force, is present only in the primary system. In [18] it is shown that the similarity fails in controlling stability of non-conservative systems loaded by follower forces, since similar controllers double the pair of the critical eigenvalues of the structure (lying on the imaginary axis) and



the gyroscopic (piezoelectric) coupling splits them, generally entailing instability. The detrimental effects of a similar controller on the stability of a generalized visco-elastic Beck's beam (see, e.g., [33, 40, 48]) are also discussed in [18] where it is also conjectured that a suitable designed non-similar PEM system could be successful in enhancing the stability performances of the beam. Control strategies for non-similar and discrete PEM systems are defined in [44], for discrete systems, and it is shown that piezoelectric controllers may successfully improve both the linear stability and the nonlinear behavior [45, 46] of the Ziegler's column [34], also in the presence of nonlinear damping [47].

Hence in this work, the performance of non-similar controllers, designed following the strategies of [44], is investigated for a continuous system, the well-known visco-elastic Beck's beam [33, 41, 40, 38], i.e. a damped cantilevered beam, loaded at the free-end by a follower force, which triggers Hopf bifurcation. For this mechanical system in [41], the effects of lumped dashpots on the linear stability are studied with the aim to increase the Hopf critical load. In this paper, the same goal is pursued by equipping the beam with distributed piezoelectric devices, that are shunted to an analogous circuit, designed as the simplest possible of those presented in [31]. An exact linear stability analysis is developed to show the effectiveness of the proposed piezoelectric control, in improving the beam stability.

The paper is organized as follows. In Sect 2. the model of the PEM system is presented. In Sect 3. an exact linear stability analysis is developed for both uncontrolled and controlled primary system. In Sect 4. the control strategies of [44] are adapted to the visco-elastic Beck's beam. In Sect 5. numerical evaluation of the stability domains is presented for different mechanical and electrical parameters. In Sect 6. concluding remarks are drawn. Finally, an Appendix, containing details on model derivation, closes the paper.

2. The Piezo-Electro-Mechanical model

A planar beam, displayed in Fig 1, is considered as the mechanical primary system. It is an Euler-Bernoulli beam, clamped at the end *A* and free at the end *B*, of length ℓ , cross-section inertia I , mass per unit-length ρ . A follower force of intensity F is applied at the beam tip *B*, thus entailing its compression in the reference rectilinear configuration. The direction of the force remains aligned with the tangent to the deflected beam axis. The beam is made of a visco-elastic material obeying the Kelvin-Voigt law, of elastic modulus E , and viscous coefficient η , which will be referred to as the 'internal damping'. It is also assumed that the beam lies on a viscous linear soil of constant c , to model the damping due to surrounding air, which will be called ahead the 'external damping'. The system here described is known in the literature as the visco-elastic Beck's beam (see, e.g., [33, 38, 36, 40, 41, 49]).

Distributed piezoelectric devices are attached to the beam (here idealized as a continuous layer bonded to the beam and covering the whole structure), and shunted to an electric circuit. This latter, sketched in Fig 1 with the box E.C., was designed in [31] to control the vibrations of non-autonomous systems: it consists in a chain of interconnected RCL elements, called there *zero-order network* and *zero-order dissipation*, namely (Z, Z) , where (\cdot, \cdot) has the meaning of the order of spatial derivatives appearing in damping- and stiffness-like terms, entering in the flux-linkage equation, as it will be clear soon. In this way a Piezo-Electro-Mechanical (PEM) system is built up.

The current state of the PEM system is described, at time t by: (i) the axial and transverse displacements of the beam, $u(s, t)$ and $v(s, t)$, respectively, and by the rotation of the beam cross-section $\vartheta(s, t) = v'(s, t)$, all referred to the initially straight configuration, $s \in [0, \ell]$ being the material abscissa and the prime denoting s -differentiation; (ii) the flux-linkage $\psi(s, t)$, which is the time primitive of the electric potential.

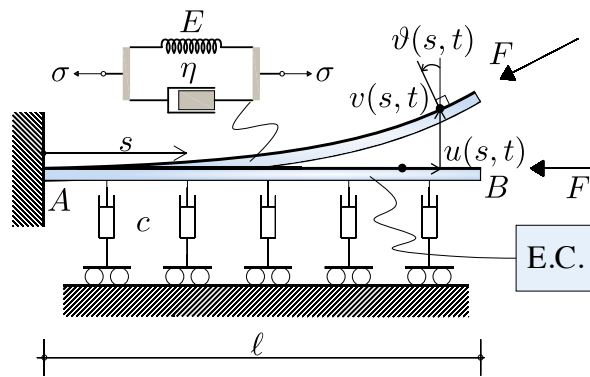


Fig. 1. Piezoelectric-controlled visco-elastic Beck's beam.

The equations of motion of the PEM are derived through the Extended Hamilton Principle (see A for details on derivation). In non-dimensional form they read:

$$\begin{aligned}
 \ddot{v} + \beta_m \dot{v} + \alpha_m v'''' + v'''' + 2\mu v'' - \gamma \dot{\psi}'' &= 0, \\
 \nu_e \ddot{\psi} + \beta_e \dot{\psi} + \kappa_e \psi + \gamma \dot{v}'' &= 0, \\
 v_A = v'_A &= 0, \\
 -v'''_B - \alpha_m v''_B + \gamma \dot{\psi}'_B &= 0, \\
 v''_B + \alpha_m \dot{v}'_B - \gamma \dot{\psi}_B &= 0,
 \end{aligned}
 \tag{1}$$

where the dot denotes t -differentiation. Equations (2)-a,b are the field equations; Eqs (2)-c and (2)-d,e are the geometrical and mechanical boundary conditions at *A* and *B*, respectively. Moreover, α_m and β_θ ($\theta = m, e$) are the non-dimensional internal and external (mechanical and electrical) damping coefficients, respectively; ν_e and κ_e are the, here referred to as, non-dimensional electrical mass and stiffness, respectively. Finally, γ is the coupling parameter and μ is the non-conservative force, which, throughout the paper, is taken as the main bifurcation parameter.



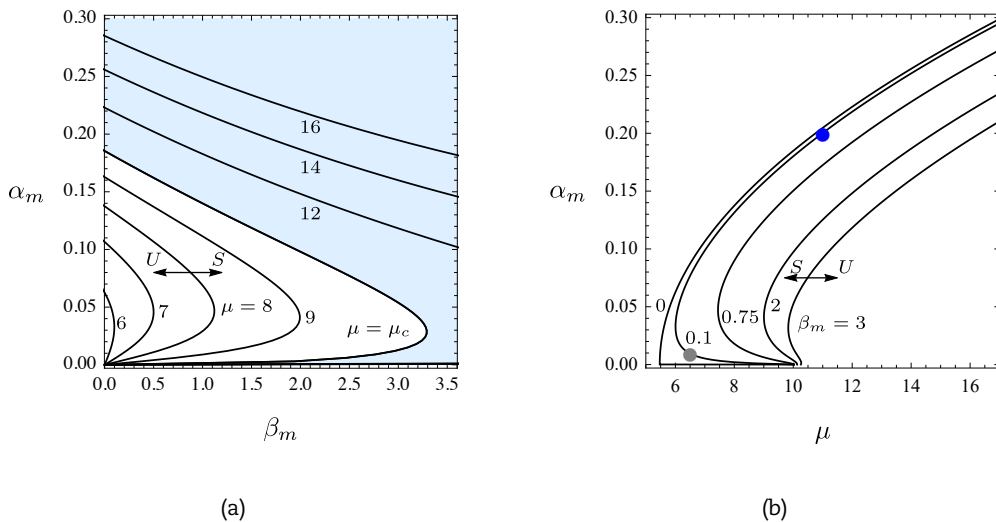


Fig. 2. Linear stability diagram for the visco-elastic Beck's beam: (a) μ -isolines in the (β_m, α_m) -plane; (b) β_m -isolines in the (α_m, μ) -plane. S stable region, U unstable region.

3. Linear stability analysis

In this section an exact linear stability analysis is carried out for the PEM system. First the problem is addressed for the uncontrolled visco-elastic Beck's beam ($\gamma = 0$) and some results of literature are recalled (the reader is referred to [48, 40, 49, 38]). Then, the analysis is developed for the whole PEM system, aiming at build up the stability domains.

3.1 The mechanical subsystem

Stability of the trivial, rectilinear configuration of the visco-elastic Beck's beam is governed by the linear eigenvalue problem, associated with Eq (1). This space boundary value problem is obtained by taking a solution in the form $v(s, t) = \hat{v}(s) e^{\lambda t}$, and by substituting it in Eq (1), that becomes:

$$\begin{aligned}
 (1 + \alpha_m \lambda) \hat{v}'''' + 2\mu \hat{v}'' + (\lambda^2 + \beta_m \lambda) \hat{v} &= 0, \\
 \hat{v}_A = \hat{v}'_A &= 0, \\
 -(1 + \alpha_m \lambda) \hat{v}'''_B &= 0, \\
 (1 + \alpha_m \lambda) \hat{v}''_B &= 0.
 \end{aligned}
 \tag{2}$$

The field equation (2)-a and the boundary conditions at the clamp A, Eq (2)-b, lead to the solution:

$$\hat{v}(s) = c_1 [\cos(ps) - \cosh(qs)] + c_2 \left[\frac{\sin(ps)}{p} - \frac{\sinh(qs)}{q} \right],
 \tag{3}$$

where $p = p(\lambda, \mu, \alpha_m, \beta_m) \in \mathbb{C}$ and $q = q(\lambda, \mu, \alpha_m, \beta_m) \in \mathbb{C}$. By enforcing the remaining boundary conditions at the free end B, an algebraic system is obtained, namely:

$$\mathbf{S}_\lambda \mathbf{c} = \mathbf{0},
 \tag{4}$$

where $\mathbf{c} := (c_1, c_2)^T$ is a vector collecting arbitrary constants, and \mathbf{S}_λ is the 'dynamic stiffness matrix' of the problem, function of the eigenvalue λ , of the control parameter μ , and of auxiliary parameters α_m, β_m , i.e. $\mathbf{S}_\lambda = \mathbf{S}_\lambda(\lambda; \mu; \alpha_m, \beta_m)$. The characteristic equation $\det \mathbf{S}_\lambda = 0$ provides the eigenvalues $\lambda = \lambda(\mu; \alpha_m, \beta_m)$; by letting $\lambda = \xi + i\omega$, with $\xi, \omega \in \mathbb{R}$, it can be written in real variables as:

$$f(\xi, \omega; \mu; \alpha_m, \beta_m) + i g(\xi, \omega; \mu; \alpha_m, \beta_m) = 0,
 \tag{5}$$

with $f, g \in \mathbb{R}$. For a given set of parameters $(\mu; \alpha_m, \beta_m)$, the system $f = 0, g = 0$ furnishes the unknowns ξ, ω . Once the eigenvalue is known, the solution of the (singular) system (4), under a proper normalization condition, gives the associated eigenfunction (3).

The (generic) Hopf bifurcation takes place at the manifold of the parameter space at which $\xi = 0, \omega \neq 0$, namely:

$$\begin{aligned}
 f(0, \omega; \mu; \alpha_m, \beta_m) &= 0, \\
 g(0, \omega; \mu; \alpha_m, \beta_m) &= 0.
 \end{aligned}
 \tag{6}$$

System (6) implicitly defines a multi-valued surface in the (μ, α_m, β_m) -space, parametrized by the frequency ω . It is important to remark that, when damping is zero, i.e. $\alpha_m = \beta_m = 0$, a circulatory system is obtained for which all the eigenvalues have zero real part (they lie on the imaginary axis). In this case, a 'circulatory' or 'reversible' Hopf bifurcation occurs at the manifold of the parameter plane on which two simple eigenvalues merge into a double eigenvalue. The manifold can no more be defined by the system (6), since the second equation is identically zero, i.e. $g(0, \omega; \mu; \alpha_m, \beta_m) \equiv 0$, hence, when this coalescence takes place, the Hopf bifurcation manifold is defined by Eq (6)-a together with $\partial f / \partial \omega = 0$ (see [48] for further details).



Linear stability diagram of the visco-elastic Beck's beam

The linear stability diagram of the uncontrolled visco-elastic Beck's beam ($\gamma = 0$) is determined by solving system (6), i.e. by evaluating the parameters combination at which a generic Hopf bifurcation takes place. No closed-form solutions of Eqs (6) can be found, but asymptotic and numerical methods can be applied. It is found (see, e.g., [40, 38]) that, when μ increases from zero, the first eigenvalue, i.e. the one having the lowest frequency, is the responsible for the loss of stability of the beam, which occurs at a critical load value μ_d (subscript d means damped system), and at critical frequency ω_d , both depending on damping.

Figure 2-a shows the linear stability diagram of the visco-elastic Beck's beam, in the (β_m, α_m) -plane, obtained by numerically solving system (6). Each contour line $\mu = \text{const}$ of Fig 2-a, belongs to the critical locus, i.e. to the slice of the surface (6) that defines the parameters combination at which the first mode of the beam manifests incipient instability. The points on the contour lines represent generic Hopf bifurcation states: on the left side of each contour line, there are unstable systems (labeled with U in Fig 2-a), while on its right side there are stable ones (labeled with S in Fig 2-a). It can be shown that (see, e.g., [36, 35, 38, 40, 39]), the critical surface also contains the μ -axis, which represents the family of undamped systems ($\alpha_m = \beta_m = 0$); these systems are marginally stable, since the eigenvalues are purely imaginary and can only move along the imaginary axis, when μ changes. The circulatory Hopf bifurcation takes place at $\mu = \mu_c \simeq 10.02$ (subscript c means circulatory), at which the first two eigenvalues collide, at a frequency ω_c , and, if μ_c is overcome, they separate, each in one of the two half-planes of the complex plane, thus entailing instability.

Figure 2-a clarifies the fact that, small internal damping α_m is detrimental in terms of beam stability, since it produces a finite lowering of the critical load from μ_c to μ_d that, in the absence of external damping β_m can be lowered up to a minimum value $\mu_d = 5.47$, below which the beam is stable for any damping combination [40]. This phenomenon is known in the literature as the 'Ziegler paradox' or the 'destabilizing effect of damping'. On the contrary, β_m has a beneficial effect on the beam stability since, for a given α_m the critical load increases with it. In particular, $\alpha_m = 0$ represents an optimal direction in the damping plane, along which, adding β_m to the system entails $\mu_d \geq \mu_c$ and $\mu_d \rightarrow \mu_c$ as $\beta_m \rightarrow 0$, i.e. no destabilizing effect exists at all. Moreover Fig 2-a shows that, when α_m is sufficiently large, it can increase the critical load μ_d , becoming stabilizing. Then, for damping parameters belonging to the region filled in light blue in Fig 2-a, the effects of the destabilization paradox are exhausted since $\mu_d > \mu_c$.

Finally, analogous considerations can be drawn by looking at Fig 2-b, where the β_m contour lines of the critical surface are displayed in the (μ, α_m) -plane. In particular, it is worth to notice that:

- for a given β_m , introducing a small α_m entails $\mu_d < \mu_c$;
- the larger is β_m , the lower is the destabilizing effect of α_m ;
- for a sufficiently large α_m , the destabilizing effect of internal damping vanishes, i.e. $\mu_d > \mu_c$;
- for a given (α_m, β_m) , the critical load μ_d increases with β_m , but it can also increase with α_m , providing it is sufficiently large.

3.2 The PEM system

Stability analysis of the PEM system is now discussed. Due to the simplicity of the adopted electric circuit, it is possible to pursue an exact solution on the same line of that carried out for the primary system.

First, the general solution of Eqs (1) is written in the form $v = \hat{v}(s) e^{\lambda t}$ and $\psi = \hat{\psi}(s) e^{\lambda t}$, thus entailing:

$$\begin{aligned}
 (1 + \alpha_m \lambda) \hat{v}'''' + 2\mu \hat{v}'' + (\lambda^2 + \beta_m \lambda) \hat{v} - \gamma \lambda \hat{\psi}'' &= 0, \\
 (\lambda^2 \nu_e + \beta_e \lambda + \kappa_e) \hat{\psi} + \gamma \lambda \hat{v}'' &= 0, \\
 \hat{v}_A = \hat{v}'_A &= 0, \\
 -(1 + \alpha_m \lambda) \hat{v}'''_B + \gamma \lambda \hat{\psi}'_B &= 0, \\
 (1 + \alpha_m \lambda) \hat{v}''_B - \gamma \lambda \hat{\psi}_B &= 0.
 \end{aligned}
 \tag{7}$$

Then, from Eq (7)-b, $\hat{\psi}(s)$ is found to be:

$$\hat{\psi} = -\frac{\gamma \lambda}{\lambda^2 \nu_e + \beta_e \lambda + \kappa_e} \hat{v}'' \tag{8}$$

By eliminating $\hat{\psi}(s)$ in Eqs (7)-a,d,e, the following eigenvalue problem is obtained:

$$\begin{aligned}
 (1 + \alpha_m \lambda + \alpha_p \lambda) \hat{v}'''' + 2\mu \hat{v}'' + (\lambda^2 + \beta_m \lambda) \hat{v} &= 0, \\
 \hat{v}_A = \hat{v}'_A &= 0, \\
 -(1 + \alpha_m \lambda + \alpha_p \lambda) \hat{v}'''_B &= 0, \\
 (1 + \alpha_m \lambda + \alpha_p \lambda) \hat{v}''_B &= 0,
 \end{aligned}
 \tag{9}$$

where:

$$\alpha_p(\lambda) := \frac{\gamma^2 \lambda}{\lambda^2 \nu_e + \beta_e \lambda + \kappa_e} \tag{10}$$

is the dissipation term due to the piezoelectric coupling and depending on the eigenvalue λ . It is apparent that, the effect of the controller is to add, to the mechanical subsystem, an internal damping-like term. In fact, the eigenvalue problem (9) is formally equivalent to that of the visco-elastic Beck's beam (9), when the substitution $\alpha_m \rightarrow \alpha_m + \alpha_p$ is performed. Therefore, Hopf bifurcation manifolds (6), can be found by following the same procedure described for the mechanical subsystem; in particular, an implicitly defined multi-valued surface in the $(\mu, \alpha_m, \beta_m, \nu_e, \kappa_e, \beta_e, \gamma)$ -space, parametrized by the frequency ω , is obtained. The slice of the surface associated with the condition of incipient instability of the eigenvalue, which first crosses from the left the imaginary axis, is the critical surface.



4. The control strategies

The target is now to conceive suitable control strategies, i.e. to design the parameters of the secondary system in such a way that the Hopf bifurcation of the PEM system takes place at a critical value of the load parameter larger than μ_d , i.e. larger than the critical load of the uncontrolled primary system. To this end, the approach adopted in [44] is followed, with the aim to find the parameters of the controller, able to maximize the electrical dissipation for given mechanical properties.

The control strategies are defined by considering the primary system loaded at $\mu = \mu_d$, assuming, as usual in applications, a small coupling γ , and by conceiving to make the following experience: (i) the controller is turned off, while the visco-elastic Beck's beam is allowed to harmonically oscillate at a certain large amplitude and with a frequency ω_d ; (ii) the controller is turned on, so that its motion is forced, via the gyroscopic coupling, by the larger response of the mechanical system; (iii) the electrical response grows up from zero and modifies the mechanical response, again through the gyroscopic coupling. In this framework, the definition of suitable control strategies consists in maximizing the response of the electrical subsystem, so that it can effectively dissipate the mechanical energy during the exchange process.

The task is accomplished by performing a straightforward expansion of the eigenvalue $\lambda_0 = \pm i\omega_d$, assuming the electrical response smaller than the mechanical one, and by searching for singularities of the solution at which an ordering violation occurs. In these singular cases, the electrical response cannot be considered small but, in contrast, it is of the same order of, or larger than, the mechanical response. Following [44], a suitable perturbation method is applied (details not reported here) to solve the eigenvalue problem (7) under the above mentioned assumptions. The coupling parameter is rescaled as $\gamma \rightarrow \varepsilon\gamma$, where $0 < \varepsilon \ll 1$ is a perturbation parameter, and eigenpairs are expanded as:

$$\begin{aligned} \lambda &= \lambda_0 + \varepsilon^2 \lambda_2 + \mathcal{O}(\varepsilon^4), \\ \hat{v} &= \hat{v}_0 + \varepsilon^2 \hat{v}_2 + \mathcal{O}(\varepsilon^4), \\ \hat{\psi} &= \varepsilon \hat{\psi}_1 + \varepsilon^3 \hat{\psi}_3 + \mathcal{O}(\varepsilon^5), \end{aligned} \tag{11}$$

consistently with the idea that the electrical response is smaller than the mechanical one. Substituting the expansions (11) into the problem (7), a chain of linear perturbation equations follows. By solving them in cascade, the following ε -order expression for the electrical amplitude is found:

$$\hat{\psi}_1 = -\frac{\gamma i \omega_d \hat{v}_0''}{(-\omega_d^2 \nu_e + i \omega_d \beta_e + \kappa_e)}, \tag{12}$$

where \hat{v}_0 is the solution of Eq (2).

An analysis of Eq (12) reveals that, by taking β_e sufficiently small, $\hat{\psi}_1$ tends to infinite or becomes of the same order of \hat{v}_0 , when the conditions which follow hold. In particular, three controllers, whose coupling to the primary system is linear and gyroscopic, can be defined (see [44] for details), namely:

- *Non-Singular (resonant) Controller (NSC)*: $\kappa_e = \mathcal{O}(1)$, $\nu_e = \mathcal{O}(1)$ and $\kappa_e/\nu_e = \omega_d^2$; moreover, $\beta_e = \mathcal{O}(\varepsilon)$;
- *Singular Non-Resonant Controller (SNRC)*: $\kappa_e = \mathcal{O}(\varepsilon)$, $\nu_e = \mathcal{O}(\varepsilon)$ and $\kappa_e/\nu_e \neq \omega_d^2$; moreover $\beta_e = \mathcal{O}(\varepsilon)$;
- *Singular Resonant Controller (SRC)*: $\kappa_e = \mathcal{O}(\varepsilon)$, $\nu_e = \mathcal{O}(\varepsilon)$ and $\kappa_e/\nu_e = \omega_d^2$; moreover, $\beta_e = \mathcal{O}(\varepsilon^{3/2})$.

It is worth to notice that each of the controllers resembles the characteristics of well-known control devices, namely: the *NSC* and the *SRC* those of the TMD, having large (*NSC*) or small (*SRC*) mass and stiffness, respectively, entailing a semi-simple (non-singular) or a defective (singular) eigenvalue at the bifurcation; the *SNRC* is close to the *NES*.

5. Numerical results

In this section, the behavior of the three controllers is analyzed by evaluating the linear stability domains of the PEM system and their dependence on the electrical parameters. To this end, an exact linear stability analysis, carried out along the lines discussed in Sect 3., is performed, with the aim to detect how the controllers affect the stability of the PEM system, and to evaluate their effectiveness in increasing the beam's critical load μ_d . The linear stability diagrams of the PEM system, are built up by evaluating the exact Hopf bifurcation loci, Eqs (6): these, for a given mechanical damping (α_m, β_m), depend on five parameters, namely $\mu, \nu_e, \kappa_e, \beta_e, \gamma$.

Two sample beams are selected, differing each other for the choice of the damping parameters. They are referred to as 'underdamped' and 'overdamped' beams, respectively, according to the role played by damping, which in the former case has a destabilizing effect with respect to the undamped system, while in the latter is stabilizing (remember Fig 2). The two cases are:

- *underdamped beam*: $\alpha_m = 0.01$ and $\beta_m = 0.1$, entailing $\mu_d = 6.46$ and $\omega_d = 5.92$, labeled with a gray bullet in Fig 2-b;
- *overdamped beam*: $\alpha_m = 0.2$ and $\beta_m = 0.1$, entailing $\mu_d = 10.99$ and $\omega_d = 5.82$, labeled with a blue bullet in Fig 2-b.

Before analyzing the quantitative effect of each controller, a preliminary linear stability analysis is presented. The aim is to clarify how the stability diagram of the uncontrolled primary system, Fig 2-b, with $\beta_m = 0.1$ (which corresponds to the definition of both the underdamped and overdamped beams) can change because of the piezoelectric control, i.e to show how α_p , defined in Eq (10), affects the beam's critical load. Clearly, this type of analysis requires a careful design of the electrical parameters for a given mechanical subsystem. The specific choice, here made for the electrical coefficients, will be justified ahead through parametric analyses.

Figure 3 shows the stability domains of the PEM system in the (μ, α_m) -plane, when $\gamma = 0.1$ and $\beta_e = 0.05, 0.25, 0.5$. The PEM system is equipped with: (i) *NSC* controller (Fig 3-a), when $\nu_e = 1, \kappa_e = \omega_d^2$; (ii) *SRC* controller (Fig 3-b), when $\nu_e = 0.1, \kappa_e = 0.1 \omega_d^2$; (iii) *SNRC* controller (Fig 3-a), when $\nu_e = 0.1, \kappa_e = 0.5$. In the same figure the boundary of the stability domain of the uncontrolled beam is represented by the black line, which actually separates the stable region S_u (on its left), from the unstable one U_u (on its right), where subscript *u* stands for uncontrolled; the stability boundaries for the controlled cases are represented by the blue lines, separating the stable region S_c (on the left of each of them) from the unstable one U_c (on the right), where subscript *c* stands for controlled.

Concerning the effect of the *NSC* on the stability of the PEM system (Fig 3-a), it is observed that, independently from the electrical damping, for small α_m (underdamped region of the stability diagram), the controller has considerable detrimental effect, since it reduces the stable region S_c , i.e. the boundaries of the controlled system are on the left of the uncontrolled one; when α_m increases



(entering the overdamped region of the stability diagram), the *NSC* can have a beneficial effect, providing a proper design of β_e . A qualitative analogous behavior is shown by the *SRC* (Fig 3-b), for which, however, a higher sensitivity to β_e is detected with respect to the *NSC*, since it can have a significant quantitative effect in reducing or enlarging the stable region of the PEM system. Finally, the *SNRC* (Fig 3-c) can have a beneficial effect on the beam's stability, independently from α_m , i.e. in both the underdamped and overdamped regions: indeed, the boundaries of the controlled system are on the right of the uncontrolled one, providing a proper choice of β_e .

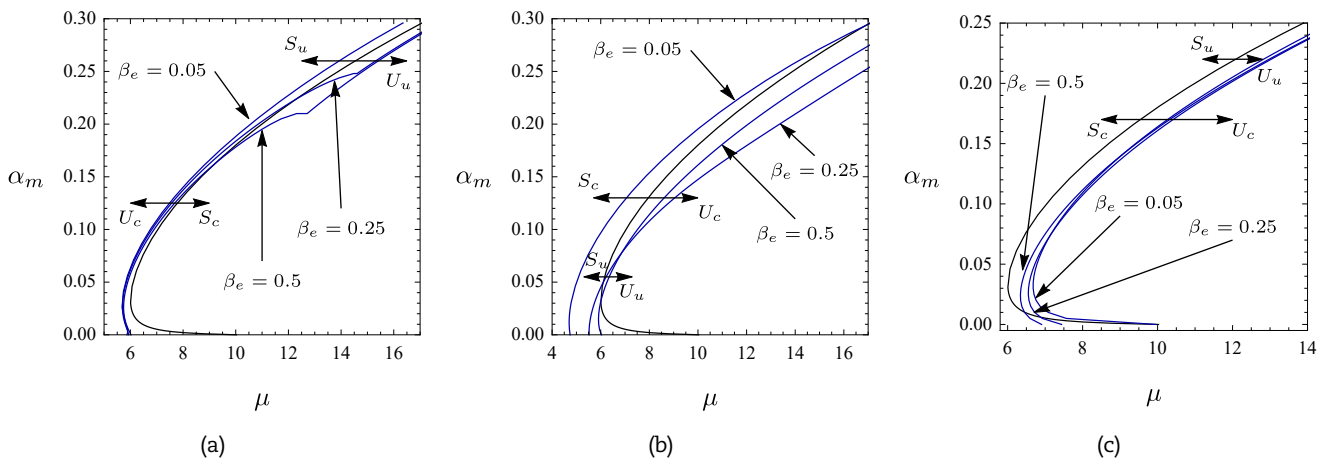


Fig. 3. Stability domains of the PEM system in the (μ, α_m) -plane, when $\gamma = 0.1$, $\beta_e = 0.05, 0.25, 0.5$ and: (a) $\nu_e = 1$ (*NSC*); (b) $\nu_e = 0.1$ (*SRC*); (c) $\nu_e = 0.1$, $\kappa_e = 0.5$ (*SNRC*). Black lines correspond to uncontrolled beam. Blue lines correspond to controlled beam. S_u, U_u denote stable and unstable regions of the uncontrolled system. S_c, U_c denote stable and unstable regions of the controlled system.

The underdamped PEM system

Attention is here focused on the performance of the controllers in the underdamped PEM system. It was observed that, at low α_m , the contribution to PEM's stability of *NSC* and *SRC* (remember Figs 3-a,b) is detrimental, independently on β_e , while the *SNRC* revealed to be effective in the underdamped region (see Fig 3-c), providing a suitable design of β_e .

The linear stability diagrams are reported in Fig 4 for the PEM system equipped with the three controllers: the Hopf bifurcation loci are represented in the $(\Delta\mu, \nu_e)$ -plane, $\Delta\mu := 100(\mu - \mu_d)/\mu_d$ being the percentage variation of the critical load of the controlled system with respect to the uncontrolled one. The coupling parameter is taken $\gamma = 0.1$ and the electrical damping is varied, namely $\beta_e = 0.05, 0.1, 0.2$. Moreover: (i) for the *NSC* (Fig 4-a), the electrical mass is varied in the range $\nu_e \in [0.5, 4]$; (ii) for the *SRC* (Fig 4-b), $\nu_e \in (0, 0.5]$; for the *SNRC* (Fig 4-c,d), the electrical mass is varied in the same range of the *SRC*, namely $\nu_e \in (0, 0.5]$, while two values of κ_e are chosen, namely $\kappa_e := \kappa_{e,1} = 0.5$ (Fig 4-c) and $\kappa_e := \kappa_{e,2} = 15$ (Fig 4-d), to avoid tuning, and to give rise to, here referred to as, *sub-resonant* and *super-resonant* controller, whose undamped electrical frequencies are, respectively, smaller and larger with respect to the mechanical one.

It is found that the *NSC* (Fig 4-a) is not able to increase the beam's critical load, disrespecting the adopted β_e , since the Hopf loci of the controlled system are on the left of the uncontrolled beam (i.e. $\Delta\mu < 0$). Therefore, in the underdamped case, the gyroscopic coupling, together with resonance, reveals to be detrimental in terms of beam stability. A very similar behavior is observed when the *SRC* controller is considered (Fig 4-b). Also in this case, it is apparent that, notwithstanding the different scaling of the parameters and the defectiveness of the eigenvalues at the bifurcation, the *SRC* qualitatively behaves as the *NSC*, namely the Hopf loci are mostly located in the stable region of the uncontrolled beam, $\Delta\mu < 0$: however, as shown in the figure, a suitable design of ν_e and β_e may allow to find limited stable regions at $\Delta\mu > 0$.

It is important to remark that the non-similar PEM system, built up with the visco-elastic Beck's beam and the (Z, Z) circuit, cannot be successfully controlled, in the underdamped case, with the resonant controllers *NSC* and *SRC*, which, indeed produce detrimental effects on the beam's stability. This behavior is not surprising, since it was also detected in [44], for a discrete non-similar PEM system, i.e. the Ziegler's column controlled with *NSC* and *SRC*. In particular, it was shown there that resonant controllers can stabilize the primary system only: (i) when they do not act on all its degrees of freedom, i.e. they are located in suitable positions; (ii) at higher values of the mechanical damping, i.e. for overdamped structures, where, however, small stabilizing regions were detected.

The last controller to be investigated is the *SNRC*. It is seen that the sub-resonant designed controller (Fig 4-c) is effective in increasing beam's stability, since, for a sufficiently large ν_e , i.e. quite close to the resonance condition, the stability boundaries are located on the right of the axis $\Delta\mu = 0$: accordingly, the stable region of the controlled system, which is on the left of each β_e -isoline and denoted with S_c , increases with respect to that of the uncontrolled one: in particular, the larger β_e the smaller the extension of the stable region S_c . Moreover, it is worth to observe that if ν_e is too large, the controller contribution becomes negligible ($\Delta\mu \rightarrow 0$). On the contrary, the smaller ν_e , the larger S_c , but, when ν_e is such that $\sqrt{\kappa_e/\nu_e}$ is too close to ω_d , the *SNRC* behaves as the *SRC*, i.e. it has a detrimental effect on the beam's stability ($\Delta\mu < 0$). Moreover, concerning the super-resonant designed controller (Fig 4-d), it is found that the stability boundaries (blue lines) appear on the left of $\Delta\mu = 0$, thus the *SNRC* has a detrimental effect, independently from β_e ; also in this case it can be seen that, close to the resonance, the behavior of the *SNRC* tends to resemble that of the *SRC* (not shown in the figure).

It is important to remark that the effectiveness of the *SNRC* depends on the ratio κ_e/ν_e . In particular, the underdamped PEM system can be controlled by the *SNRC*, quite far from the resonance, i.e. $\kappa_e/\nu_e \neq \omega_d^2$, and in sub-resonant condition, i.e. $\sqrt{\kappa_e/\nu_e} < \omega_d$. However, if κ_e/ν_e is taken too far from ω_d^2 , the resulting piezoelectric control may become negligible.

In order to complete the investigation about the effectiveness of the *SNRC*, the stability boundaries of the underdamped PEM system are evaluated: (i) in the $(\Delta\mu, \kappa_e)$ -plane, when $\gamma = 0.1$, $\nu_e = 0.1$ and $\beta_e = 0.05, 0.1, 0.2$, Fig 5-a; (ii) in the $(\Delta\mu, \beta_e)$ -plane, when $\nu_e = 0.1$, $\kappa_e = 0.5$ (sub-resonant controller) and $\gamma = 0.1, 0.15, 0.2$, Fig 5-b. It is found that the larger κ_e the higher the load increment (see Fig 5-a), but, on the other hand, it is necessary to avoid the resonance-induced detrimental effects, according to what discussed above. Moreover, it is seen that β_e must be taken as small as possible, since when it increases, a reduction of the load increment is



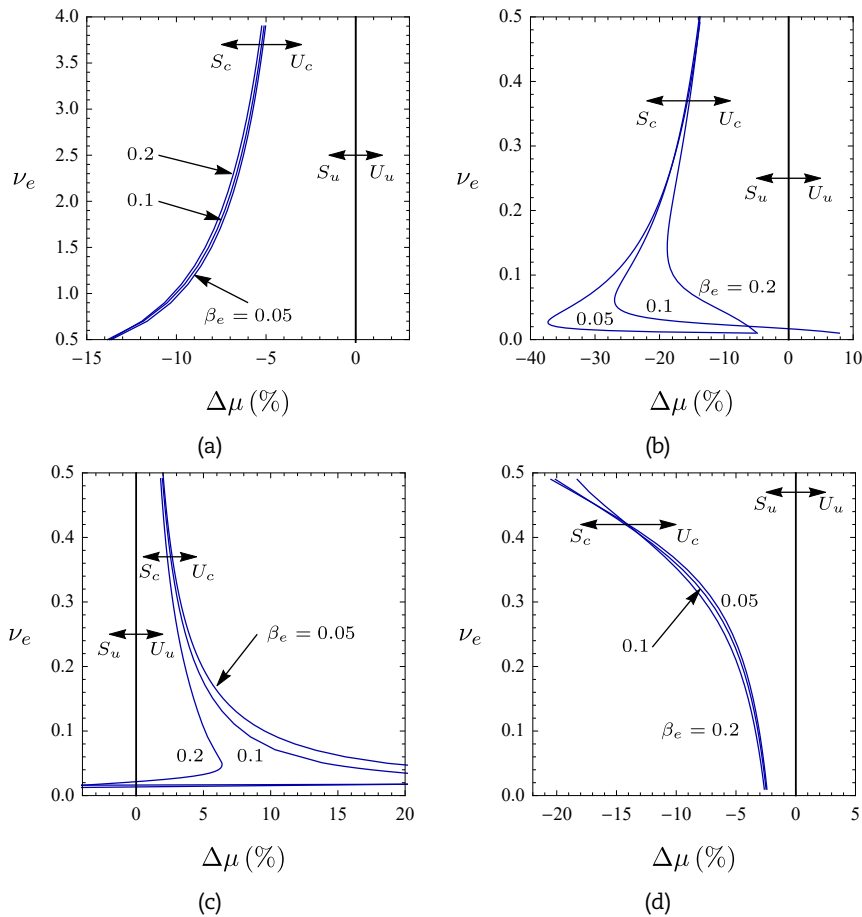


Fig. 4. Stability domains of the underdamped PEM system in the $(\Delta\mu, \nu_e)$ -plane, when $\gamma = 0.1$ and $\beta_e = 0.05, 0.1, 0.2$: (a) *NSC*; (b) *SRC*; (c), (d) *SNRC* when $\kappa_{e,1} = 0.5$ and $\kappa_{e,2} = 15$, respectively. S_u, U_u denote stable and unstable regions of the uncontrolled system. S_c, U_c denote stable and unstable regions of the controlled system.

detected. This effect can be better observed in Fig 5-b, i.e. in the $(\Delta\mu, \beta_e)$ -plane: indeed, when β_e is sufficiently small, considerably large load increments are detected, but when it is close to zero, $\Delta\mu$ can be very small or negative. The curve cusp in Fig 5-b denotes a change of the eigenvalue which triggers instability. Finally, it is seen in Fig 5-b that, when β_e is sufficiently large, the piezoelectric contribution becomes negligible, and when γ increases, the piezoelectric control becomes more effective.

The overdamped PEM system

The stability analysis is developed here to evaluate the performance of the controllers in the overdamped PEM system. It was observed that, at large α_m , the behavior of *NSC* and *SRC* depends on a suitable design of β_e (remember Figs 3-a,b), while the effectiveness of *SNRC* revealed to be less sensitive to β_e (see Fig 3-c).

As previously done, the linear stability diagrams are shown in Fig 6, for the three controllers, in the $(\Delta\mu, \nu_e)$ -plane, when $\gamma = 0.1$ and $\beta_e = 0.05, 0.1, 0.2$. The same ranges of ν_e , adopted for the underdamped case, are selected.

The behavior of the *NSC* (Fig 6-a) is close to that observed in the underdamped case, when β_e is sufficiently small, i.e. the controller has a detrimental effect; however, if a sufficiently large β_e is selected, small stable regions at $\Delta\mu > 0$ may be also found. Moreover, it is found that the *SRC* (Fig 6-b) is much more effective in the overdamped case, since large load increments arise for suitably designed β_e : again, it is seen that β_e must be sufficiently small, since, the stable region reduces when β_e becomes too large, i.e. the controller is ineffective. It is important to remark that these results confirm what found in [44], i.e. non-similar and overdamped PEM systems may be successfully controlled also by resonant controllers (*NSC, SRC*).

The effect of the *SNRC* in the overdamped PEM system is quite similar to that of the underdamped case, in both sub-resonant (Fig 6-c) and super-resonant (Fig 6-d) designed controllers. Indeed, stable regions are found at $\Delta\mu > 0$, when $\kappa_e = \kappa_{e,1}$ (Fig 6-c), and, close to the resonance, the effectiveness of the controller is maximized. However, differently from the underdamped case, here: (i) the regions in which $\Delta\mu < 0$ are negligible and detected for very small β_e ; (ii) the electrical damping can be optimized (i.e. not the smallest possible like in the underdamped case, remember Fig 5-b), in order to maximize the load increment. Moreover, in the super-resonant case, when $\kappa_e = \kappa_{e,2}$ (Fig 6-d), the *SNRC* has mostly a detrimental effect: this confirms what already found in the underdamped case, but, here, when the *SNRC* approaches the resonance, i.e. it resembles the *SRC*, and for sufficiently large β_e , it becomes effective in stabilizing the PEM system.

In order to better understand the performance of the *NSC* and *SRC* in the overdamped PEM system, the stability domains in the $(\Delta\mu, \beta_e)$ -plane are shown in Fig 7, when $\gamma = 0.1, 0.15, 0.2$. In particular, Fig 7-a is referred to *NSC*, when $\nu_e = 1$, while Fig 7-b is relevant to the *SRC*, when $\nu_e = 0.1$. It is seen that at low values of β_e , both the *NSC* and *SRC* are detrimental in terms of stability, i.e. $\Delta\mu < 0$, but stabilization is possible when β_e increases; however, when β_e is too large, a reduction of the stable regions, which tend to that of the uncontrolled beam ($\Delta\mu = 0$), is experienced. Therefore, it can be seen that an optimal value of β_e exists which for a given magnitude of the coupling parameter γ , maximizes the load increment. Again, it is found that the effectiveness of the control increases with the coupling parameter. It is important to highlight that, when a curve cusp is encountered in Fig 7, a change of the mode which triggers instability of the PEM system manifests itself.



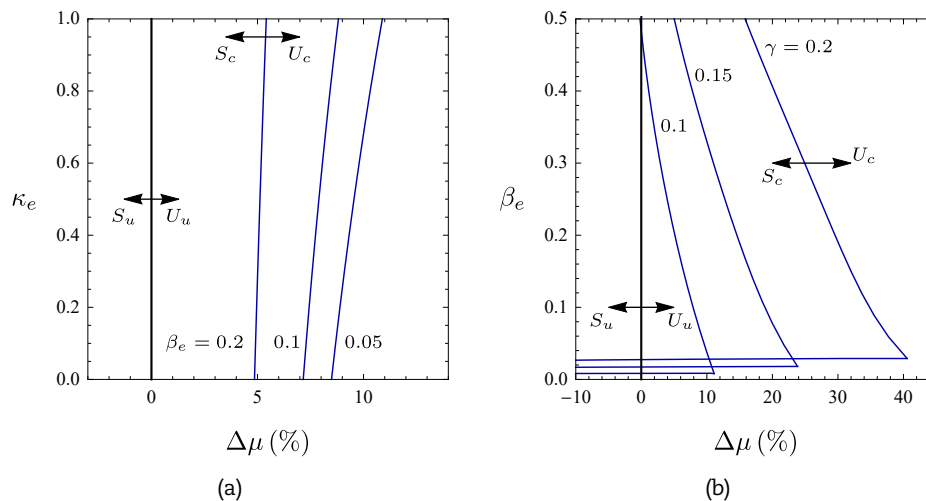


Fig. 5. Stability domains of the underdamped PEM system equipped with *SNRC*: (a) β_e -isolines in the $(\Delta\mu, \kappa_e)$ -plane, when $\nu_e = 0.1$ and $\gamma = 0.1$; (b) γ -isolines in the $(\Delta\mu, \beta_e)$ -plane, when $\nu_e = 0.1$ and $\kappa_e = 0.5$. S_u, U_u denote stable and unstable regions of the uncontrolled system. S_c, U_c denote stable and unstable regions of the controlled system.

Finally, the stability domains of the overdamped PEM system, equipped with *SNRC* are shown in Fig 8, by adopting the same electrical parameters of the underdamped case (remember Fig 5). In particular in Fig 8-a the linear stability diagram is displayed in the $(\Delta\mu, \kappa_e)$ -plane, while in Fig 8-b it is shown in the $(\Delta\mu, \beta_e)$ -plane. Similarly to what observed in the underdamped case, the stability of the PEM system slightly improves when κ_e increases, see Fig 8-a. Moreover, also for the *SNRC* an optimal value for the electrical damping may be designed to maximize the load increment, see Fig 8-b: indeed, β_e allows an increase of the Hopf load until it exceeds a threshold above which the load increment reduces, tending to that of the uncontrolled beam. It is remarked that, $\beta_e = 0$ is out of the range of Fig 8-b to avoid, as already observed in the underdamped case, that the PEM system encounters the Hopf bifurcation at $\Delta\mu < 0$ (see Fig 5-b). Also in this case, the larger γ , the larger the beneficial effect of the controller.

6. Conclusions

Control strategies for the visco-elastic Beck's beam, suffering from Hopf bifurcation due to the presence of a follower force, have been proposed in this paper. Distributed piezoelectric patches, shunted to the so-called (Z, Z) electric circuit, have been taken as the control device. The equations of motion, governing the resulting non-similar Piezo-Electro-Mechanical (PEM) system, have been derived through the Extended Hamilton Principle. The exact solution of the eigenvalue problem has been worked out for the PEM system. An asymptotic analysis revealed the possibility to adopt three different controllers, recently developed for discrete PEM systems, in which the mechanical and electrical subsystems are coupled by small terms of gyroscopic nature. An exact linear stability analysis has been carried out to show the effectiveness of the controllers in improving the linear stability of the visco-elastic Beck's beam, for different mechanical damping parameters, giving rise to an underdamped and overdamped system. A parametric analysis has also been developed to detect the role played by each of the electrical parameters. The following conclusions are drawn.

1. The overall effect of the designed piezoelectric control is to add an internal damping-like term, function of the eigenvalue, to the primary system: the destabilizing effect due to the (mechanical) internal damping, can be mitigated by properly governing the magnitude of the piezoelectric damping.
2. The resonant controllers, namely *NSC* and *SRC*, are detrimental in terms of stability of the underdamped PEM system, irrespectively from the magnitude of electrical damping: indeed, as it occurs when the controller is similar, the secondary system doubles the pair of the critical eigenvalues and the gyroscopic coupling splits them, generally causing Hopf bifurcation at a critical load lower than that of the uncontrolled system. Moderately extended stable regions may be found for the overdamped PEM system, when the electrical damping is suitably designed.
3. The non-resonant controller, namely *SNRC*, successfully works in improving the linear stability of the underdamped PEM system, provided that its undamped frequency is sufficiently smaller than the critical frequency of the beam. In this case the smaller is the electrical damping, the higher is the beneficial effect. The *SNRC* is effective also in the overdamped case, where an optimal value of electrical damping, which maximizes the critical load increment has been numerically detected.
4. A suitable design of the *SNRC* may effectively improve the linear stability of the visco-elastic Beck's beam. However, a careful sensitivity analysis is required to avoid detrimental effects caused by resonance and to properly design the electrical damping parameter.
5. The effectiveness of the controllers, in all the analyzed cases, increases with the magnitude of the gyroscopic coupling.

The study allowed to investigate the effectiveness of the proposed piezoelectric controller in enhancing the linear stability of the Beck's beam. Further investigations may be conducted to analyze the post-critical scenarios that the controlled beam may experience when endowed with such controller and investigate its effectiveness in mitigating the limit-cycle oscillations arising beyond the Hopf critical load. Another interesting aspect is to consider more complex controllers, i.e. different analog circuits, to investigate their effect on a richer PEM system stability.

Author Contributions

Arnaldo Casalotti and Francesco D'Annibale contributed equally to this work. Francesco D'Annibale conceived the scientific idea of this paper. Arnaldo Casalotti and Francesco D'Annibale developed analytical solutions and carried out numerical simulations.



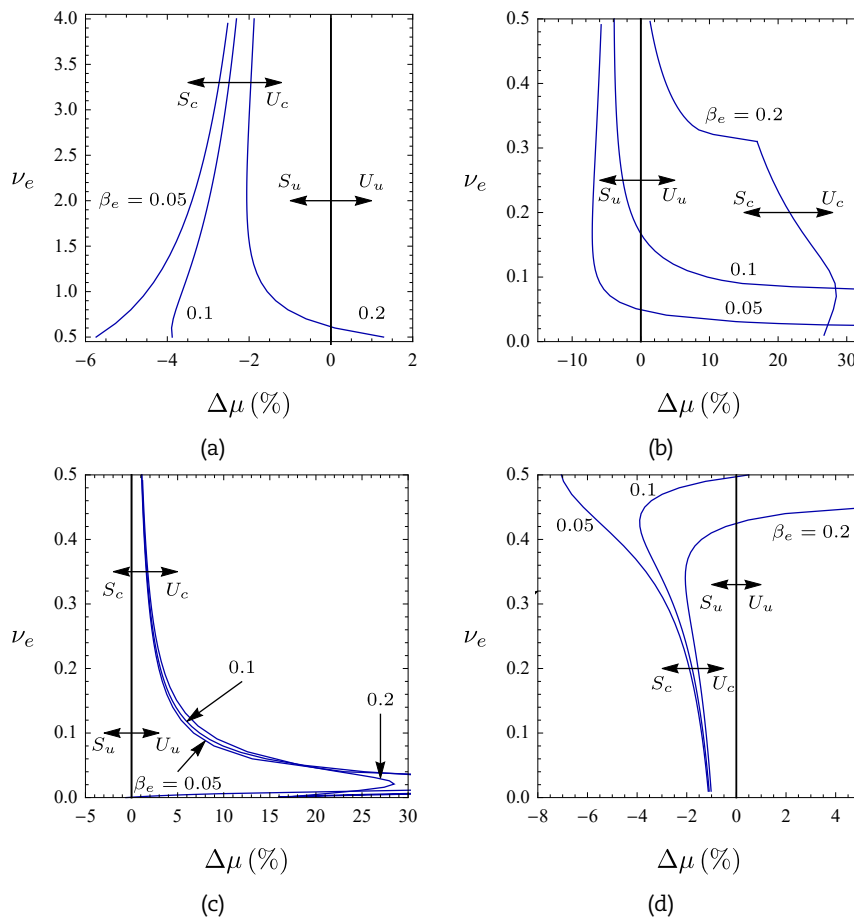


Fig. 6. Stability domains of the overdamped PEM system in the $(\Delta\mu, \nu_e)$ -plane, when $\gamma = 0.1$ and $\beta_e = 0.05, 0.1, 0.2$: (a) NSC; (b) SRC; (c), (d) SNRC when $\kappa_{e,1} = 0.5$ and $\kappa_{e,2} = 15$, respectively. S_u, U_u denote stable and unstable regions of the uncontrolled system. S_c, U_c denote stable and unstable regions of the controlled system.

The manuscript was written through the contribution of both the authors. All authors discussed the results, reviewed and approved the final version of the manuscript.

Conflict of Interest

The authors declared no potential conflicts of interest with respect to the research, authorship and publication of this article.

Funding

The authors received no financial support for the research, authorship and publication of this article.

References

- [1] Frahm, H., Device for damping vibrations of bodies, 1911, US Patent 989,958.
- [2] Den Hartog, J.P., *Mechanical vibrations*, Courier Corporation, 1985.
- [3] Yamaguchi, H., Harnpornchai, N., Fundamental characteristics of multiple tuned mass dampers for suppressing harmonically forced oscillations, *Earthquake engineering & structural dynamics*, 1993, 22(1), 51–62.
- [4] Abé, M., Fujino, Y., Dynamic characterization of multiple tuned mass dampers and some design formulas, *Earthquake engineering & structural dynamics*, 1994, 23(8), 813–835.
- [5] Kareem, A., Kline, S., Performance of multiple mass dampers under random loading, *Journal of structural engineering*, 1995, 121(2), 348–361.
- [6] Rana, R., Soong, T., Parametric study and simplified design of tuned mass dampers, *Engineering structures*, 1998, 20(3), 193–204.
- [7] Gattulli, V., Di Fabio, F., Luongo, A., Simple and double hopf bifurcations in aeroelastic oscillators with tuned mass dampers, *Journal of the Franklin Institute*, 2001, 338(2-3), 187–201.
- [8] Gattulli, V., Di Fabio, F., Luongo, A., One to one resonant double Hopf bifurcation in aeroelastic oscillators with tuned mass damper, *Journal of Sound and Vibration*, 2003, 262(2), 201–217.
- [9] Gattulli, V., Di Fabio, F., Luongo, A., Nonlinear tuned mass damper for self-excited oscillations, *Wind and Structures*, 2004, 7(4), 251–264.
- [10] Ubertini, F., Prevention of suspension bridge flutter using multiple tuned mass dampers, *Wind and Structures*, 2010, 13(3), 235–256.
- [11] Vigiúé, R., Tuning methodology of nonlinear vibration absorbers coupled to nonlinear mechanical systems, Ph.D. thesis, PhD Thesis, 2010.
- [12] Casalotti, A., Arena, A., Lacarbonara, W., Mitigation of post-flutter oscillations in suspension bridges by hysteretic tuned mass dampers, *Engineering Structures*, 2014, 69, 62–71.
- [13] Gendelman, O.V., Gourdon, E., Lamarque, C.H., Quasiperiodic energy pumping in coupled oscillators under periodic forcing, *Journal of Sound and Vibration*, 2006, 294(4-5), 651–662.
- [14] Gourdon, E., Alexander, N.A., Taylor, C.A., Lamarque, C.H., Pernot, S., Nonlinear energy pumping under transient forcing with strongly nonlinear coupling: Theoretical and experimental results, *Journal of sound and vibration*, 2007, 300(3-5), 522–551.
- [15] Vakakis, A.F., Gendelman, O.V., Bergman, L.A., McFarland, D.M., Kerschen, G., Lee, Y.S., *Nonlinear targeted energy transfer in mechanical and structural systems*, vol. 156, Springer Science & Business Media, 2008.



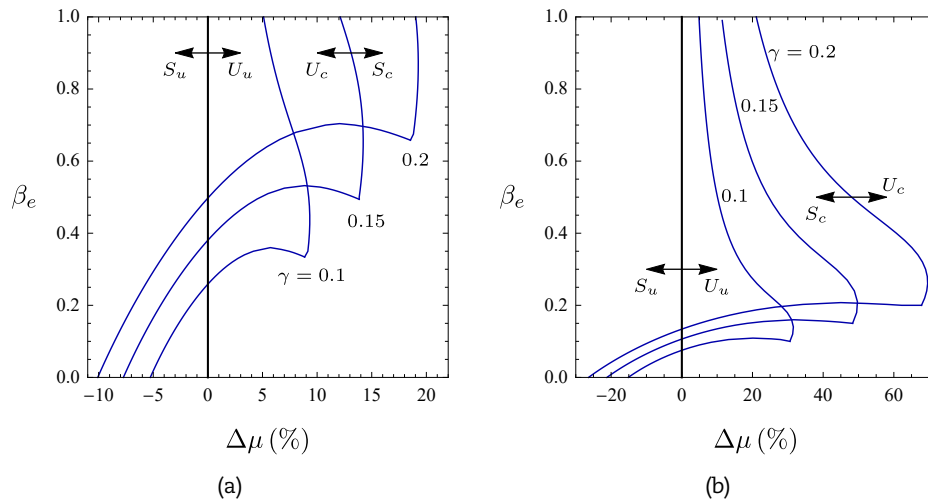


Fig. 7. Stability domains of the overdamped PEM in the $(\Delta\mu, \beta_e)$ -plane, when $\gamma = 0.1, 0.15, 0.2$ and: (a) $\nu_e = 1$ (NSC); (b) $\nu_e = 0.1$ (SRC). S_u, U_u denote the stable and unstable regions of the uncontrolled system. S_c, U_c denote the stable and unstable regions of the controlled system.

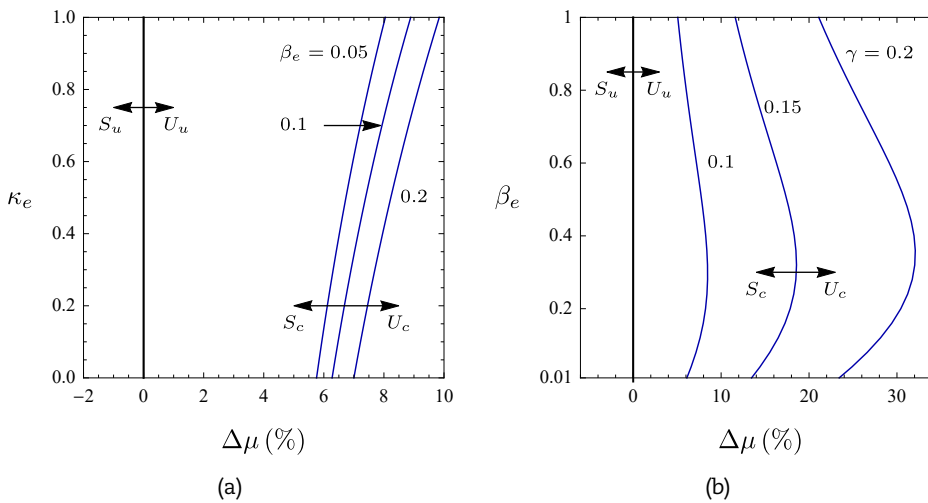


Fig. 8. Stability domains of the underdamped PEM system equipped with SNRC: (a) β_e -isolines in the $(\Delta\mu, \kappa_e)$ -plane, when $\nu_e = 0.1$ and $\gamma = 0.1$; (b) γ -isolines in the $(\Delta\mu, \beta_e)$ -plane, when $\nu_e = 0.1$ and $\kappa_e = 0.5$. S_u, U_u denote the stable and unstable regions of the uncontrolled system. S_c, U_c denote the stable and unstable regions of the controlled system.

[16] Luongo, A., Zulli, D., Dynamic analysis of externally excited nes-controlled systems via a mixed multiple scale/harmonic balance algorithm, *Nonlinear Dynamics*, 2012, 70(3), 2049–2061.

[17] Luongo, A., Zulli, D., Aeroelastic instability analysis of nes-controlled systems via a mixed multiple scale/harmonic balance method, *Journal of Vibration and Control*, 2014, 20(13), 1985–1998.

[18] D’Annibale, F., Rosi, G., Luongo, A., On the failure of the ‘similar piezoelectric control’ in preventing loss of stability by nonconservative positional forces, *Zeitschrift für angewandte Mathematik und Physik*, 2015, 66(4), 1949–1968.

[19] Del Vescovo, D., Giorgio, I., Dynamic problems for metamaterials: review of existing models and ideas for further research, *International Journal of Engineering Science*, 2014, 80, 153–172.

[20] Giorgio, I., Galantucci, L., Della Corte, A., Del Vescovo, D., Piezo-electromechanical smart materials with distributed arrays of piezoelectric transducers: current and upcoming applications, *International Journal of Applied Electromagnetics and Mechanics*, 2015, 47(4), 1051–1084.

[21] Pagnini, L.C., Piccardo, G., The three-hinged arch as an example of piezomechanic passive controlled structure, *Continuum Mechanics and Thermo-dynamics*, 2016, 28(5), 1247–1262.

[22] Alessandrini, S., Andreaus, U., dell’Isola, F., Porfiri, M., A passive electric controller for multimodal vibrations of thin plates, *Computers and Structures*, 2005, 83(15), 1236–1250.

[23] Andreaus, U., dell’Isola, F., Porfiri, M., Piezoelectric passive distributed controllers for beam flexural vibrations, *Journal of Vibration and Control*, 2004.

[24] Alessandrini, S., dell’Isola, F., Porfiri, M., A revival of electric analogs for vibrating mechanical systems aimed to their efficient control by PZT actuators, *International Journal of Solids and Structures*, 2002, 39(5295–5324).

[25] Alessandrini, S., Andreaus, U., dell’Isola, F., Porfiri, M., Piezo-electromechanical (pem) kirchhoff-love plates, *European Journal of Mechanics A/Solids*, 2004, 23, 689–702.

[26] dell’Isola, F., Porfiri, M., Vidoli, S., Piezo-electromechanical (PEM) structures: passive vibration control using distributed piezoelectric transducers, *Comptes Rendus de l’Academie des Sciences, Mécanique*, 2003, 331, 69–76.

[27] dell’Isola, F., Santini, E., Vigilante, D., Purely electrical damping of vibrations in arbitrary PEM plates: A mixed non-conforming FEM-Runge-Kutta time evolution analysis, *Archive of Applied Mechanics*, 2003, 73(1-2), 26–48.

[28] dell’Isola, F., Maurini, C., Porfiri, M., Passive damping of beam vibrations through distributed electric networks and piezoelectric transducers: prototype design and experimental validation, *Smart Materials and Structures*, 2004, 13(2), 299.

[29] Porfiri, M., dell’Isola, F., Frattale Mascioli, F., Circuit analog of a beam and its application to multimodal vibration damping, using piezoelectric transducers, *International Journal of Circuit Theory and Applications*, 2004, 32(4), 167–198.

[30] Rosi, G., Control of sound radiation and transmission by means of passive piezoelectric networks: modelling, optimization and experimental implementation, Ph.D. thesis, Sapienza University of Rome, University of Paris 6, 2010.

[31] Maurini, C., dell’Isola, F., Del Vescovo, D., Comparison of piezoelectronic networks acting as distributed vibration absorbers, *Mechanical Systems and Signal Processing*, 2004, 18(5), 1243–1271.



- [32] Bolotin, V.V., *Nonconservative problems of the theory of elastic stability*, Macmillan, New York, 1963.
- [33] Beck, M., Die Knicklast des einseitig eingespannten, tangential gedrückten Stabes, *Zeitschrift für angewandte Mathematik und Physik ZAMP*, 1952, 3(3), 225–228.
- [34] Ziegler, H., Die Stabilitätskriterien der elastomechanik, *Ingenieur Archiv*, 1952, 20(1), 49–56.
- [35] Seyranian, A., Mailybaev, A., *Multiparameter stability theory with mechanical applications*, vol. 13, World Scientific, Singapore, 2003.
- [36] Kirillov, O.N., *Nonconservative stability problems of modern physics*, Walter de Gruyter, Berlin/Boston, 2013.
- [37] Kirillov, O.N., A theory of the destabilization paradox in non-conservative systems, *Acta Mechanica*, 2005, 174(3-4), 145–166.
- [38] Kirillov, O., Seyranian, A., The effect of small internal and external damping on the stability of distributed non-conservative systems, *Journal of Applied Mathematics and Mechanics*, 2005, 69(4), 529–552.
- [39] Luongo, A., D'Annibale, F., A paradigmatic minimal system to explain the Ziegler paradox, *Continuum Mechanics and Thermodynamics*, 2015, 27(1-2), 211–222.
- [40] Luongo, A., D'Annibale, F., On the destabilizing effect of damping on discrete and continuous circulatory systems, *Journal of Sound and Vibration*, 2014, 333(24), 6723–6741.
- [41] D'Annibale, F., Ferretti, M., Luongo, A., Improving the linear stability of the beck's beam by added dashpots, *International Journal of Mechanical Sciences*, 2016, 110, 151–159.
- [42] Wang, Q., Quek, S.T., Enhancing flutter and buckling capacity of column by piezoelectric layers, *International Journal of Solids and Structures*, 2002, 39(16), 4167–4180.
- [43] Wang, Y., Wang, Z., Zu, L., Stability of viscoelastic rectangular plate with a piezoelectric layer subjected to follower force, *Archive of Applied Mechanics*, 2012, 83(4), 495–507.
- [44] D'Annibale, F., Rosi, G., Luongo, A., Linear stability of piezoelectric-controlled discrete mechanical systems under nonconservative positional forces, *Meccanica*, 2015, 50(3), 825–839.
- [45] D'Annibale, F., Rosi, G., Luongo, A., Controlling the limit-cycle of the ziegler column via a tuned piezoelectric damper, *Mathematical Problems in Engineering*, 2015, 2015.
- [46] D'Annibale, F., Rosi, G., Luongo, A., Piezoelectric control of hopf bifurcations: A non-linear discrete case study, *International Journal of Non-Linear Mechanics*, 2016, 80, 160–169.
- [47] D'Annibale, F., Piezoelectric control of the hopf bifurcation of ziegler's column with nonlinear damping, *Nonlinear Dynamics*, 2016, 86(4), 2179–2192.
- [48] Luongo, A., D'Annibale, F., Double zero bifurcation of non-linear viscoelastic beams under conservative and non-conservative loads, *International Journal of Non-Linear Mechanics*, 2013, 1–12.
- [49] Luongo, A., D'Annibale, F., Nonlinear hysteretic damping effects on the post-critical behaviour of the visco-elastic beck's beam, *Mathematics and Mechanics of Solids*, 2017, 22(6), 1347–1365.

ORCID iD

Arnaldo Casalotti  <https://orcid.org/0000-0002-9047-9523>

Francesco D'Annibale  <https://orcid.org/0000-0002-6580-9586>



© 2021 by the authors. Licensee SCU, Ahvaz, Iran. This article is an open access article distributed under the terms and conditions of the Creative Commons Attribution-NonCommercial 4.0 International (CC BY-NC 4.0 license) (<http://creativecommons.org/licenses/by-nc/4.0/>)

How to cite this article: Arnaldo Casalotti, Francesco D'Annibale. Improving the linear stability of the visco-elastic Beck's beam via piezoelectric controllers, *J. Appl. Comput. Mech.*, 7(SI), 2021, 1098-1109. <https://doi.org/10.22055/JACM.2020.33648.2260>

Appendix A Model derivation

To derive the equations of motion, the same variational methodology of [18], to which the reader is referred to, is followed. There, a meta-model of a PEM system was formulated through a variational approach and by enforcing similarity between the mechanical and electrical subsystems, such that the electrical subsystem could have the same spectral properties of the primary system. As a result the dynamical behavior of the PEM was governed by mechanical and electrical partial differential equations having the same structure and proportional coefficients.

In the variational framework of [18], the following assumptions are made in the present paper.

1. The principle of similarity is not enforced in the derivation of the PEM model.
2. Linear configuration-dependent actions, i.e. follower forces, act in the system but, differently from [18], only on the mechanical subsystem.
3. Linear kinematics is assumed for the beam and its axial behavior is not taken into account in what follows.
4. Linear velocity-dependent actions are considered in the PEM system, both of mechanical (damping) and electric (resistivity) nature. In particular: (i) the external dissipation is considered in both the mechanical and electrical subsystems, where it is proportional to the mass and resistance operators, respectively; (ii) the internal dissipation, derived by adopting a Kelvin-Voigt visco-elastic constitutive law, is taken into account only in the mechanical subsystem.
5. The adopted electric circuit is the so-called (Z, Z) of [31].
6. The mass and stiffness of piezoelectric devices, due to their smallness, are considered negligible.

In a first step, internal dissipation and external actions are neglected, so that the system can be described only in terms of its Lagrangian $L := L_m + L_e + L_p$, where subscripts m, e, p refer to the mechanical, electrical and piezoelectric part, respectively. Then, in the $[t_1, t_2]$ interval, the first variation of the action functional is evaluated as:

$$\delta H := \int_{t_1}^{t_2} \delta (L_m + L_e + L_p) dt = \delta H_m + \delta H_e + \delta H_{em}, \quad (13)$$

where $\delta H_m, \delta H_e$ and δH_{em} are the mechanical, electrical and electro-mechanical contributions, respectively. The third step is to take into account for non-conservative actions, pumping into or extracting energy from the PEM system. To this end, the Extended Hamilton Principle is adopted, namely:



$$\delta \tilde{H} := \delta H + \delta W_m + \delta W_e = 0, \tag{14}$$

for any kinematically admissible field of variations. In Eq (14), $\delta W_m, \delta W_e$ are the works expended by non-conservative actions (subscripts m and e refer to mechanical and electrical works, respectively).

Under the above mentioned assumptions, $\delta H_m, \delta W_m$ and δH_{em} read:

$$\begin{aligned} \delta H_m &= \int_{t_1}^{t_2} \left[\int_0^\ell (\rho \dot{v} \delta \dot{v} - EI v'' \delta v'') \, ds \right] dt, \\ \delta W_m &= - \int_{t_1}^{t_2} \left[\int_0^\ell (c \dot{v} \delta v + \eta I \dot{v}'' \delta v'' + F v'' \delta v) \, ds \right] dt, \\ \delta H_{em} &= \int_{t_1}^{t_2} \left[\int_0^\ell E_{em} (\dot{\psi} \delta v'' - \dot{v}'' \delta \psi) \, ds \right] dt. \end{aligned} \tag{15}$$

Equations (15)-a is the first variation of the action functional of the Euler-Bernoulli beam; Eq (15)-b is the nonconservative work done by mechanical (external and internal) damping forms and by the external action F ; Eq (15)-c defines the piezoelectric electro-mechanical coupling, of gyroscopic type, governed by the coupling coefficient E_{em} .

The electrical contribution to the action functional (14) is given by the piezoelectric devices, shunted to the (Z, Z) electrical circuit: this is idealized as an array of infinite in-parallel RCL elements (see [31]). Accordingly, δH_e and δW_e read:

$$\begin{aligned} \delta H_e &:= \int_{t_1}^{t_2} \int_0^\ell \left(C \dot{\psi} \delta \dot{\psi} - \frac{1}{L} \psi \delta \dot{\psi} \right) \, ds dt, \\ \delta W_e &:= - \int_{t_1}^{t_2} \int_0^\ell \frac{1}{R} \dot{\psi} \delta \psi \, ds dt, \end{aligned} \tag{16}$$

where C, L and R are linear densities of piezoelectric capacitance, of circuit inductance and resistance, respectively.

The variational principle (14) supplies the following equations of motion for the PEM system:

$$\begin{aligned} \rho \ddot{v} + c \dot{v} + \eta I \dot{v}'''' + EI v'''' + F v'' - E_{em} \dot{\psi}'' &= 0, \\ C \ddot{\psi} + \frac{1}{R} \dot{\psi} + \frac{1}{L} \psi + E_{em} \dot{v}'' &= 0. \end{aligned} \tag{17}$$

The problem is completed by initial conditions (assuming the system at rest) and by the following set of boundary conditions of geometric type at the clamped end A :

$$v_A = v'_A = 0, \tag{18}$$

and of mechanical type at the free end B :

$$\begin{aligned} -EI v'''_B - \eta I \dot{v}'''_B + E_{em} \dot{\psi}'_B &= 0, \\ EI v''_B + \eta I \dot{v}''_B - E_{em} \dot{\psi}_B &= 0. \end{aligned} \tag{19}$$

Finally, by introducing $\tilde{t} = t/t_0, \tilde{s} = s/\ell, \tilde{v}(\tilde{s}, \tilde{t}) = v/v_0$ and $\tilde{\psi}(\tilde{s}, \tilde{t}) = \psi/\psi_0$, as the non-dimensional time, abscissa, displacement and flux-linkage, respectively, the non-dimensional form of Eqs (17), (18) and (19) is that of Eqs (1) (tilde removed), where the following definitions hold:

$$\begin{aligned} t_0 &:= \ell^2 \sqrt{\frac{\rho}{EI}}, & \psi_0 &= \sqrt{\frac{\rho}{C_0}} v_0, & \alpha_m &= \frac{\eta I}{\ell^2 \sqrt{\rho EI}}, \\ \beta_m &= \frac{c \ell^2}{\sqrt{\rho EI}}, & \mu &= \frac{F \ell^2}{2EI}, & \nu_e &= \frac{C}{C_0}, \\ \beta_e &= \ell^2 \sqrt{\frac{\rho}{EI}} \frac{1}{C_0 R}, & \kappa_e &= \frac{\rho \ell^4}{EI} \frac{1}{C_0 L}, & \gamma &= \frac{E_{em}}{\sqrt{C_0 EI}} \end{aligned} \tag{20}$$

and in which t_0, v_0 and ψ_0 are the characteristic time, displacement and flux-linkage, respectively, and C_0 is a scaling capacitance.

